

Design of Chemical Sensor Arrays for Monitoring Disposal Sites on the Ocean Floor

Aleksandar Jeremić, *Student Member, IEEE*, and Arye Nehorai, *Fellow, IEEE*

Abstract—We develop methods for automatic environmental monitoring of disposal sites on the deep ocean floor using chemical sensor arrays and statistical hypothesis testing. Such sites have been proposed to relocate dredge materials from harbors and shipping channels. The transport of pollutants is modeled as a diffusion process, and the measurement and statistical models are derived by exploiting the spatial and temporal evolution of the associated concentration distribution. We derive two detectors, the generalized likelihood ratio (GLR) test and the mean detector, and determine their performance in terms of the probabilities of false alarm and detection. The results are applied to the design of chemical sensor arrays satisfying criteria specified in terms of these probabilities, and to optimally select a number of sensors and time samples. Numerical examples are used to demonstrate the applicability of our results.

Index Terms—Chemical sensing, environmental monitoring, pollutant detection, sensor array processing.

I. INTRODUCTION

THE CONTINUOUS buildup of sediment in U.S. ports and harbors has a detrimental impact upon national economic and military security. Dredging is required to maintain channel depths; however, dredged material may contain considerable quantities of contaminated sediment and waste materials. It has recently been proposed to dispose of the dredged materials by depositing them in bags on the abyssal ocean seafloor. This proposal is called the deep ocean relocation (DOR) program (see [1]). As a result of the presence of contaminants in the dredged material, environmental monitoring of pollutants near the disposal sites must be performed. In this paper (see also [2]), we develop procedures for automatic monitoring of the disposal sites using chemical sensor arrays and statistical hypothesis testing. We derive algorithms for detecting the presence of pollutants outside the sites and design sensor arrays for optimal detection performance. This work extends our previous results in [3].

In Section I-A, we discuss the problem background and consider physical phenomena that affect pollutant transport in the ocean. In Section II, we develop mathematical models of transport processes for the DOR scenario. In Section III,

we derive the spatio-temporal measurement model of the sensor array, assuming sensors that are selective to a particular substance. We develop two detection algorithms: the first is a generalized likelihood ratio (GLR) test [4] and the second is a mean detector that uses averaged measurements. The GLR detector utilizes prior information by employing physical models of diffusion and gives superior performance when these models are reasonably accurate. On the other hand, the mean detector is useful when very little is known about the transport mechanisms but at the expense of reduced detection performance. We determine the detection probability (P_d) and false alarm probability (P_{fa}) of these detectors for use as performance measures. In Section IV, we propose methods for optimum array design, including the choice of the number of sensors, time samples, and array size. Numerical examples are presented throughout to demonstrate the applicability of our results.

Although our work is developed in the context of the DOR problem, all the results can easily be extended to different environments, such as open air.

A. Problem Background

According to the DOR plan [1], the dredged material is enclosed in geotextile bag-like cylindrical containers, each with a volume of about 800 yd³. A transporter disposes of 20 such units per trip. The disposal location is chosen to be a region in which the ocean bottom is topographically flat with a low kinetic energy floor. Due to some randomness that exists in the free fall of the bags, their points of impact with the bottom will be scattered. However, the bag locations after impact will be measured, and we therefore assume that these locations are known.

Each bag may contain a mixture of different pollutants, see, for example, [5], where characteristic pollutant concentration levels in dredged materials from the ports of New York and New Jersey are given. Typical pollutants found are metals (cadmium, chromium, copper, etc.), PAH's (anthracene, benzo pyrene, fluorene, etc.), PCB's, pesticides, and petroleum. The level of concentration for a particular pollutant may be very small, for example, pesticide concentrations in this example are below 0.01 ppm.

A fraction of the bags may leak or rupture upon impact with the bottom. The dispersed material will form an apron deposit located in both the near field, which is the area where all the bags are to be deposited, likely to be 5 km in diameter, and the midfield, which is the larger area that will receive dispersed sediment and is around 10 km in diameter. Beyond

Manuscript received December 12, 1997; revised April 28, 1998. This work was supported by the Defense Advanced Research Projects Agency, Program Element 63226E, by the Air Force Office of Scientific Research under Grant F49620-97-1-0481, by the National Science Foundation under Grant MIP-9615590, and by the Office of Naval Research under Grant N00014-98-1-0542. This paper was approved for publication by Associate Editor Robert C. Spindel.

The authors are with the Department of Electrical Engineering and Computer Science, University of Illinois at Chicago, Chicago, IL 60607 USA.

Publisher Item Identifier S 0364-9059(98)05298-4.

the midfield, the ambient bottom is defined as the far field, and compliance [6] requires that concentration levels of the contaminants must be insignificant in this region. For the remainder of the paper, we assume that the sensor array will be located in the midfield area with a diameter in the range 5–10 km.

The dredged spoil may enter the water column primarily in two phases, namely as small particles or dissolved materials. Unless turbidity flow occurs, the spread of the particles will be confined to a relatively small area, see [7] and hence will not be considered in this paper. However, the dissolved materials will remain in suspension much longer and may be carried away by larger scale processes of advection and diffusion.

There are two basic situations that may create plume of the dissolved materials. The first is bag impact, and the second is water exchange between the pore waters within the deposit and the overlaying water column. However, we will not consider continuous release since its effects are negligible compared with that of impulsive sources over the time interval of interest (see [8]). We will consider several phenomena that affect the dispersion of released plumes: molecular diffusion, advective and turbulent flow, and bioturbation.

II. TRANSPORT MODELS

In this section, we describe the physical models of underwater substance transport. The transport is mathematically described as a diffusion process by appropriate differential equations (see [9]) to which other effects are added.

A. Molecular Diffusion

Small-scale spreading of substances is governed by a mixing process, often called molecular diffusion. Molecular diffusion is caused by random displacements of molecules of dissolved or suspended substances. The process is predictable and exactly described by the well-known Fick's law of diffusion

$$\mathbf{f}(\mathbf{r}, t) = -\mathcal{K}\nabla c(\mathbf{r}, t) \quad (2.1)$$

where $\mathbf{f}(\mathbf{r}, t)$ is the flux density vector, in units of $\text{kg}/\text{m}^2\cdot\text{s}$, at a point \mathbf{r} and time t , $c(\mathbf{r}, t)$ is the diffusing substance concentration in units of kg/m^3 , and \mathcal{K} is a matrix of diffusivity coefficients in units of m^2/s . Okubo [9] provides an excellent discussion of diffusion processes in the oceans and the reader is referred to his work for a thorough summary. Following [9], we assume, for simplicity, that the principal axes of the diffusivity tensor coincide with horizontal and vertical coordinate axes. Then \mathcal{K} has the diagonal form

$$\mathcal{K} = \begin{bmatrix} \kappa_x & 0 & 0 \\ 0 & \kappa_y & 0 \\ 0 & 0 & \kappa_z \end{bmatrix}. \quad (2.2)$$

For a source-free volume, by the continuity equation [10] we have

$$\frac{\partial c}{\partial t} = -\nabla \cdot \mathbf{f}. \quad (2.3)$$

Combining (2.1)–(2.3) we get, for a source-free volume and space-invariant diffusivity, the well-known diffusion equation

$$\frac{\partial c}{\partial t} = \kappa_x \frac{\partial^2 c}{\partial x^2} + \kappa_y \frac{\partial^2 c}{\partial y^2} + \kappa_z \frac{\partial^2 c}{\partial z^2}. \quad (2.4)$$

To model the seafloor environment, we use a semi-infinite medium bounded by an infinitely large plain. Assuming that the distances at which measurements are taken are much larger than the source (bag) dimensions, we use a point source model. Thus, we consider a point source at \mathbf{r}_0 in a semi-infinite medium, releasing a diffusing substance at a time-varying rate of $\mu(t)$ kg/s , starting at time t_0 (time of impact).

In order to solve (2.4), it is necessary to transform the coordinates and reduce the problem to a corresponding problem in an isotropic medium. We use the following transformation (see [10]):

$$K = \begin{bmatrix} \sqrt{\frac{\kappa}{\kappa_x}} & 0 & 0 \\ 0 & \sqrt{\frac{\kappa}{\kappa_y}} & 0 \\ 0 & 0 & \sqrt{\frac{\kappa}{\kappa_z}} \end{bmatrix} \quad (2.5)$$

where κ is a constant that may be chosen arbitrarily, for example, $\kappa = (\kappa_x \kappa_y \kappa_z)^{1/3}$.

After this transformation, the solution of (2.4), detailed in Appendix A, can be formulated as a convolution of the rate of release and the concentration distribution that would result from an instantaneous release of a unit amount of substance, i.e.,

$$c(\mathbf{r}, t) = \int_0^{t-t_0} \frac{\mu(t-t_0-\tau)}{(4\pi\kappa\tau)^{3/2}} \exp\left\{-\frac{|\mathbf{r}'-\mathbf{r}'_0|^2}{4\kappa\tau}\right\} d\tau \quad (2.6)$$

where $\mathbf{r}' = K\mathbf{r}$, and $\mathbf{r}'_0 = K\mathbf{r}_0$. The convolution in (2.6) can be computed analytically in only a few cases, when the source is a constant rate or impulsive (instantaneous), for example.

Although the above solution applies to molecular diffusion, it can approximate other phenomena as well. Turbulent diffusion is often approximated as molecular diffusion [9], but with larger diffusivities, so-called eddy diffusivities, with typical values anywhere from 10^2 to 10^{10} times as big as molecular diffusivity. Since turbulent diffusion dominates molecular diffusion, we will use the expression molecular diffusion to denote turbulent diffusion that can be modeled as (2.6) with \mathcal{K} corresponding to eddy diffusivities.

Similarly, the redistribution of sediment particulates by organisms, or bioturbation, can also be approximately modeled as a diffusion process (see [11]), assuming that the redistribution is done by large numbers of organisms and is spread over a large number of individual transport events. However, this phenomenon is negligible if turbulent or advective flows are present.

B. Advective Diffusion

Advection corresponds to fluid flow on a relatively large scale that typically consists of mean flow and fluctuations that are periodic and nonperiodic. Such flows strongly affect the

transportation of dissolved/suspended material by enhancing the exchange of material at the interface of the deposited substance and water.

Currents near the ocean bottom are the principal means of advection. The definition of the mean and fluctuating parts of the motion requires a separation between these parts that depends upon the question at hand [12]. In general, the mean-flow field is defined by the averaging time or space scale which is appropriate for a particular problem. For candidate DOR disposal sites, the average (over small-scale motions) of the mean flow is expected to be in the range of 0–4 cm/s.

The periodic fluctuations are caused by several processes. In the abyssal ocean, the principal periodic fluctuations are due to tidal processes and to a lesser extent the natural oscillatory modes of the basin and gravitational waves. For simplicity, we consider only tidal motion, consisting of a lunar component (see [13]), having the form

$$\mathbf{v}(t) = v_x \cos\left(\frac{2t}{P}\right) + v_y \sin\left(\frac{2t}{P}\right) + \bar{\mathbf{v}} \quad (2.7)$$

where v_x and v_y are the tidal velocity amplitudes in the horizontal directions, P is the tidal period, and $\bar{\mathbf{v}}$ is the mean-flow velocity. Note that (2.7) corresponds to a velocity vector whose tip traces out an ellipse.

To include the mean flow and tidal effects in the underwater diffusion model, we consider a more general diffusion equation

$$\frac{\partial c}{\partial t} = \text{div}(\mathcal{K}\nabla \cdot c) - \nabla \cdot c(\mathbf{v}(t)). \quad (2.8)$$

The solution of (2.8), detailed in Appendix B, is obtained similarly to (2.4) and is given by

$$c(\mathbf{r}, t) = \int_0^{t-t_0} \frac{\mu(t-t_0-\tau)}{(4\pi\kappa\tau)^{3/2}} \cdot \exp\left\{-\frac{|\mathbf{r}' - \mathbf{v}(\tau)\tau - \mathbf{r}'_0|^2}{4\kappa\tau}\right\} d\tau. \quad (2.9)$$

1) Impulsive Source: An impulsive source is due to initial stirring up of previously deposited material or to instantaneous release of substances from bags ruptured upon impact. The resulting impact plume can be approximately modeled as an impulsive source at time t_0 of strength μ in kilogram units. Substituting $\mu(t) = \mu\delta(t-t_0)$ in (2.9) yields

$$c(\mathbf{r}, t) = \frac{\mu}{(4\pi\kappa(t-t_0))^{3/2}} \cdot \exp\left\{-\frac{|\mathbf{r} - \mathbf{v}(t-t_0)(t-t_0) - \mathbf{r}_0|^2}{4\kappa(t-t_0)}\right\}. \quad (2.10)$$

C. Numerical Examples of Concentration Distributions

To investigate the effects of the aforementioned phenomena, we compute the concentration distribution for various scenarios. In all examples, unless otherwise stated, we use realistic (eddy) diffusivity coefficients $\kappa_h = \kappa_x = \kappa_y = 10 \text{ m}^2/\text{s}$ and $\kappa_v = \kappa_z = 10^{-4} \text{ m}^2/\text{s}$ (see [14]).

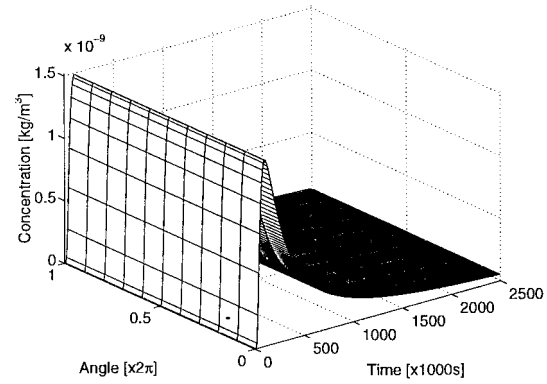


Fig. 1. Concentration distribution at radius $r = 2500$ m, single source.

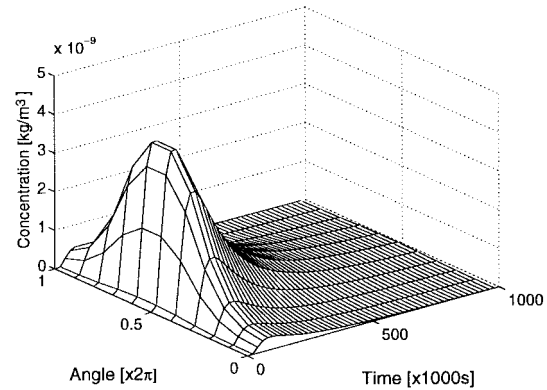


Fig. 2. Concentration distribution at radius $r = 2500$ m with a mean-flow single source.

1) Single Source: In this section we illustrate the concentration distribution due to molecular diffusion and advective flow. We present results for an impulsive source [see (2.10)], located at $\mathbf{r}_0 = (0, 0, 0)$ with a normalized release rate of $\mu = 1 \text{ kg}$ (realistic value will be used as part of the DOR simulation below).

Fig. 1 shows the spatio-temporal evolution of the concentration for a single impulsive source, as a function of azimuthal angle and time, at a radius of $r = 2500$ m. It can be seen that the dispersion is spatially independent since there is no advection. The concentration distribution in Fig. 2 illustrates the same results but with a mean flow of magnitude $v = 1 \text{ cm/s}$. Note that the concentration levels are higher than in the previous example. This is true in particular in an angular range around the downstream direction. As a result of the increased concentration levels, the detection performance is expected to be better.

2) DOR Scenario—Multiple Sources: In this section, we simulate the concentration distribution for a scenario typical of the DOR program. We use 20 sources (bags) spatially distributed with two-dimensional (2-D) Gaussian distribution. If the fall trajectory is erratic, the landing pattern will approximate a circular Gaussian distribution. Otherwise, if it is smooth and stable, the landing pattern approximates a Rayleigh distribution (see [15]). We will only consider impact plumes that can be modeled as impulsive sources (see Section II-B) (note that between each transporter's 20 bag deposition,

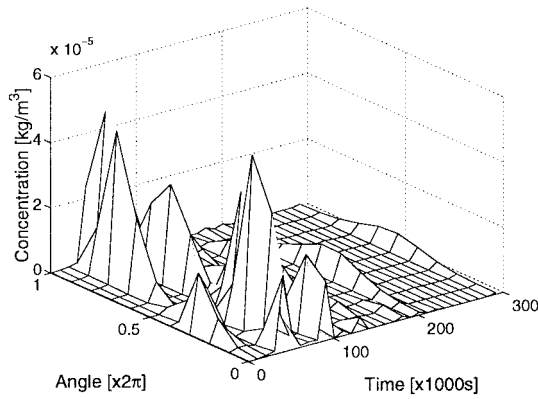


Fig. 3. Concentration distribution for 20 impulsive sources (one run) at radius $r = 2500$ m.

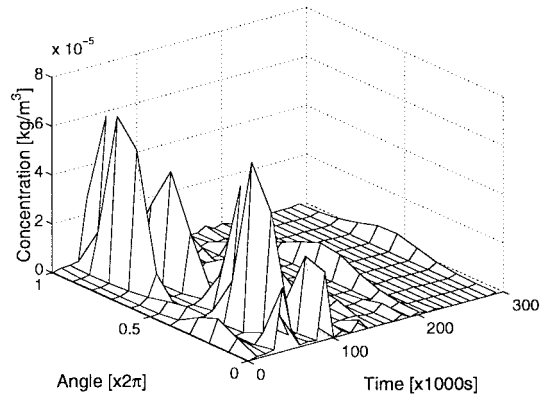


Fig. 4. Concentration distribution for 20 impulsive sources, averaged over 10000 runs, at radius $r = 2500$ m.

plumes will be driven primarily by exchange processes between pore waters and the overlaying water column that can be modeled as continuous sources, however, these sources will not be considered in this paper, see Section I-A).

It has been shown [16] that the expected impulsive release after impact is 10%–15% of each bag's contents. However, only about 5% of the bag's contents will be subject to advection since the more dense component of the plume will settle out very quickly. Thus, to model the release rate for each bag, we use a β distribution with parameters 1 and 19, so that the distribution function has a peak at a release rate of 5%. Since each bag contains a mixture of different pollutants we assume that the mass of a particular pollutant is 1% of the bag contents and hence that 0.05% is the most probable value of release rate. The density of released plumes is expected to be in the range 1100–1700 kg/m³. Since we consider only materials with density similar to the water density, the density is set to $\rho = 1100$ kg/m³. For instance, using the above scenario, the most probable (according to the β distribution) release of a particular pollutant would be approximately 336 kg.

The advective flow in the DOR scenario is due to a mean flow of magnitude 1 cm/s and a tidal current that rotates directionally with a period of 12.42 h and magnitude in the range 2–5 cm/s. For illustrational purposes we will assume that the direction of the mean flow coincides with x axis.

Figs. 3 and 4 illustrate the concentration for this scenario with impulsive sources (2.10) using one run and averaging (over source locations and intensities) of 10000 runs, respectively, using the same parameters as in the previous section. In both examples, we include a mean flow of magnitude $v = 1$ cm/s and tidal flow of $v_x = 2$ cm/s and $v_y = 5$ cm/s. Observe that the only noticeable difference is that the averaged concentration distribution is more spread around the mean flow direction.

III. DETECTION AND PARAMETER ESTIMATION

A. Measurement Model

To model the measurements, we suppose a spatially distributed array of m chemical sensors located at known positions $\{\mathbf{r}_i, 1 \leq i \leq m\}$. We assume that these chemical sensors

are selective, i.e., they are sensitive only to the substance of interest. The response of each sensor is

$$y(\mathbf{r}_i, t_k) = c(\mathbf{r}_i, t_k) + b + e(\mathbf{r}_i, t_k) \quad (3.11)$$

where $c(\mathbf{r}_i, t)$ denotes the concentration of the substance (pollutant) of interest, b denotes a bias term invariant in space and time, and $e(\mathbf{r}_i, t)$ is the measurement noise. The bias represents the sensor's response to interfering substances and concentrations resulting from previous deposits that have reached steady state. We will assume that b is known since it can be measured before the monitoring phase with high accuracy, thus its affect will be removed from the measurement model by subtraction. The time samples will be assumed to be taken at uniformly spaced time points $\{t_k = kT_s, 1 \leq k \leq p\}$, where T_s is the sampling interval and p is the number of time samples.

We lump the measurement model (3.11) into a matrix form. Without the bias

$$\mathbf{y} = A(\boldsymbol{\theta})\boldsymbol{\mu} + \mathbf{e} \quad (3.12)$$

where \mathbf{y} is an (mp) -dimensional measurement vector, $A(\boldsymbol{\theta})$ is an $mp \times n$ -dimensional source-to-sensor transfer matrix, $\boldsymbol{\theta}$ is a vector of unknown source and medium parameters, $\boldsymbol{\mu} = [\mu_1, \dots, \mu_n]^T$ is a vector of source intensities, n is the number of sources, and \mathbf{e} is a vector of measurement noise.

The transfer matrix $A(\boldsymbol{\theta})$ is given by

$$A(\boldsymbol{\theta}) = [\mathbf{a}(\boldsymbol{\theta}_1) \cdots \mathbf{a}(\boldsymbol{\theta}_n)] \quad (3.13)$$

where $\mathbf{a}(\boldsymbol{\theta}_j)$ is an (mp) -dimensional vector whose $(m(k-1) + i)$ th component is the concentration at location \mathbf{r}_i and time t_k arising from a unit-rate release from the j th pollutant source (bag). For instance, for the point source model (2.10), this element is

$$\frac{1}{(4\pi\kappa(t-t_0))^{3/2}} \exp\left\{-\frac{|\mathbf{r} - \mathbf{v}(t-t_0)(t-t_0) - \mathbf{r}_0|^2}{4\kappa(t-t_0)}\right\}. \quad (3.14)$$

The measurement noise in (3.12) corresponds to sensor noise, ambient noise, and possibly incorrect modeling. We will assume that it is uncorrelated in time and space and Gaussian distributed with zero mean and unknown variance σ^2 . Note

that, since the concentration has a nonnegative value, the Gaussian assumption is only an approximation that becomes more valid as the signal-to-noise ratio (SNR) increases. We have shown that this assumption becomes valid for SNR larger than 3 dB (see [17]).

For the remainder of the paper we will consider the case of known medium characteristics, i.e., the diffusivity matrix \mathcal{K} , velocity $\mathbf{v}(t)$, starting time of diffusion t_0 , and source locations are all known *a priori*. This is a reasonable assumption since these characteristics can be measured (as will be done according to the DOR plan [1]).

In the model (3.12), we implicitly assumed that the signal level is above the sensor sensitivity threshold. In practice, actual sensors are not reliable below a certain sensitivity threshold and, hence, unless the threshold is small, the above model will not be valid. Therefore, the design has to include a selection of sensors with sensitivity threshold sufficiently small so that the time interval in which the concentration level is above the sensitivity threshold will be large enough. Our results indicate that the sensors' sensitivity has to be at least particles per billion (ppb) to guarantee that the detection performance will not be degraded by the sensitivity threshold. In the following discussion, we will assume that sensitivity threshold does not affect the detection performance. For a detailed discussion, the reader is referred to [17].

B. Source Detection

The detection of pollutant leakage from the disposal site can be expressed as a binary decision between two hypotheses:

- H_0 : only the bias term and noise are present;
- H_1 : the source is present as well, i.e., pollutant leakage occurs from some bags.

This hypotheses formulation tests $\mu_j > 0$ for some j , versus $\mu_j = 0$ for all j . However, it can be easily modified for testing whether the source intensities (and hence the concentration levels) are above a certain value. Note that μ_j corresponds to the strength of the j th source.

1) *GLR Detector (Known Physical Model)*: The generalized likelihood ratio test (GLR) is a commonly used technique when the statistical model of measurements is determined by a parameter vector that can be estimated from the measurements [18]. This detector is based on the assumption that the solution (2.9) approximates the physical processes reasonably well and that uncertainties in the model are due mainly to measurement noise.

Under H_0 and H_1 and the above assumptions, the measurement vector is Gaussian distributed as follows:

- H_0 : $\mathbf{y} \sim \mathcal{N}[0, \sigma^2 \mathbf{I}]$;
- H_1 : $\mathbf{y} \sim \mathcal{N}[A\boldsymbol{\mu}, \sigma^2 \mathbf{I}]$, where $\mu_j \geq 0$ for $j = 1, \dots, n$.

We have omitted the dependence of A on $\boldsymbol{\theta}$ since all the medium parameters and source locations are assumed to be known.

The GLR test is given by the ratio

$$\text{GLR} = \frac{\sup_{\mu_j \geq 0, \sigma^2 > 0} \{\text{likelihood}(\mathbf{y})\}}{\sup_{\mu_j = 0, \sigma^2 > 0} \{\text{likelihood}(\mathbf{y})\}} \quad (3.15)$$

where the numerator (denominator) on the r.h.s. corresponds to the likelihood function under H_1 (H_0) and is given by

$$\text{likelihood}(\mathbf{y}) = (2\pi\sigma^2)^{-mp/2} \cdot \exp \left\{ -\frac{1}{2\sigma^2} (\mathbf{y} - A\boldsymbol{\mu})^T (\mathbf{y} - A\boldsymbol{\mu}) \right\}. \quad (3.16)$$

The maximum-likelihood (ML) estimates $\hat{\boldsymbol{\mu}}$ of the source intensities under H_1 are computed as follows [19]. Let

$$\begin{aligned} \tilde{\boldsymbol{\mu}} &= [\tilde{\mu}_1, \dots, \tilde{\mu}_n]^T \\ &= (A^T A)^{-1} A^T \mathbf{y}. \end{aligned} \quad (3.17)$$

Then,

$$\hat{\boldsymbol{\mu}} = [\hat{\mu}_1, \dots, \hat{\mu}_n]^T \quad (3.18)$$

$$\hat{\mu}_j = \begin{cases} 0, & \tilde{\mu}_j \leq 0 \\ \mathbf{g}_j^T A_l^T \mathbf{y}, & \tilde{\mu}_j > 0 \end{cases} \quad (3.19)$$

where \mathbf{g}_j is the j th column of matrix $(A_l A_l^T)^{-1}$, A_l is an $mp \times l$ dimensional submatrix of matrix A whose columns correspond to positive estimates, and $\tilde{\mu}_j > 0$ (l is the number of positive components in $\tilde{\boldsymbol{\mu}}$).

The ML estimates of σ^2 are

$$\hat{\sigma}^2 = \begin{cases} \frac{1}{mp} (\mathbf{y} - A\hat{\boldsymbol{\mu}})^T (\mathbf{y} - A\hat{\boldsymbol{\mu}}), & \text{under } H_1 \\ \frac{1}{mp} \mathbf{y}^T \mathbf{y}, & \text{under } H_0. \end{cases} \quad (3.20)$$

Inserting the ML estimates $\hat{\boldsymbol{\mu}}$ and $\hat{\sigma}^2$ into the likelihood ratio (3.15), we get

$$\text{GLR} = \left(\frac{\mathbf{y}^T \mathbf{y}}{\mathbf{y}^T \mathbf{y} - \mathbf{y}^T P_{A_l} \mathbf{y}} \right)^{mp/2} \quad (3.21)$$

where $P_{A_l} = A_l (A_l^T A_l)^{-1} A_l^T$ is the projection matrix onto the column space of A_l .

Applying the monotonic transformation $(mp/l)(x^{2/mp} - 1)$, we redefine the GLR as

$$\text{GLR} = \frac{mp}{l} \frac{\mathbf{y}^T P_{A_l} \mathbf{y}}{\mathbf{y}^T \mathbf{y} - \mathbf{y}^T P_{A_l} \mathbf{y}}. \quad (3.22)$$

The detection decision is then made by comparing the GLR in (3.22) with a threshold τ : if $\text{GLR} > \tau$, accept H_1 , otherwise H_0 .

We determine the threshold τ to yield a desired probability of false alarm P_{fa} (typically $P_{fa} = 5\%$), following the standard approach in the detection literature [4], [20]. Thus, computation of τ requires knowledge of the probability distribution of GLR under H_0 . In this case, the GLR has a central F distribution with l and $mp - l$ degrees of freedom, $F_{l, mp-l}$, where l is the number of positive components of the vector $\tilde{\boldsymbol{\mu}}$, see, e.g., [21]. Similarly, under H_1 , the GLR has a noncentral F distribution with noncentrality factor $\lambda = \boldsymbol{\mu}^T A^T A \boldsymbol{\mu} / \sigma^2$ and the same degrees of freedom.

Let L denote the random variable corresponding to l , the number of positive components in $\tilde{\boldsymbol{\mu}}$. Thus L is of lattice type and takes values $0, 1, \dots, n$ with probability $\Pr\{L = l\} = c_l$ where c_l is the probability that any l estimates of the release rates are positive. The expressions for c_l are given in Appendix B.

Although the distribution of the GLR cannot be computed in closed form, the performance measures can be expressed as sums of cumulative central and noncentral F distribution functions and are given by (see Appendix C)

$$P_{\text{fa}} = \sum_{l=1}^n c_l \{1 - \Pr[F_{l, mp-l}(0) \leq \tau]\} \quad (3.23)$$

$$P_{\text{d}} = \sum_{l=1}^n c_l \{1 - \Pr[F_{l, mp-l}(\lambda) \leq \tau]\}. \quad (3.24)$$

2) *Mean Detector (Unknown Physical Model)*: The mean detector makes less assumptions than the GLR about the model, hence it is useful when a reliable model is not available. In our case, it can be expressed as a test between the following hypotheses:

- H_0 : \mathbf{y} is distributed as $\mathcal{N}[0, \sigma^2 I]$;
- H_1 : \mathbf{y} is distributed as $\mathcal{N}[\boldsymbol{\xi}, \sigma^2 I]$.

$\boldsymbol{\xi}$ is the unknown measurement mean corresponding to concentrations due to a pollutant of interest, i.e., $\boldsymbol{\xi} = A\boldsymbol{\mu}$.

This detector is computed using the statistic (see [22, pp. 265–271])

$$T = \frac{\sqrt{N}}{mp} \frac{1}{\sqrt{\mathbf{y}_0^T \mathbf{y}_0}} \sum_{i=1}^{mp} y_i \quad (3.25)$$

where y_i is the i th component of the measurement vector \mathbf{y} , the vector \mathbf{y}_0 is a measurement vector obtained before the detection phase (in the absence of any signal), and N is the number of time samples used to obtain \mathbf{y}_0 .

Under H_0 , T has Student's central t distribution with N degrees of freedom (see [23]). Under H_1 , T has a noncentral t distribution with N degrees of freedom and noncentrality factor $\lambda = [(1/mp) \sum_{i=1}^{mp} \xi_i]^2 / \sigma^2$ (see [23]).

The performance measures are given by

$$P_{\text{fa}} = 1 - \Pr[t_N(0) \leq \tau] \quad (3.26)$$

$$P_{\text{d}} = 1 - \Pr[t_N(\lambda^2) \leq \tau] \quad (3.27)$$

where $t_N(\cdot)$ denotes the t cumulative distribution with N degrees of freedom and noncentrality factor in parentheses, and τ is the decision threshold.

C. Numerical Examples of Detection Performance

We present numerical examples to demonstrate the performance of the above detectors. We also illustrate the effects of different transport phenomena (mean flow, advection, etc.) In all these examples, the thresholds are chosen to yield a probability of false alarm $P_{\text{fa}} = 5\%$.

We define the SNR as the ratio of the squared peak value of averaged concentration distribution (see Section II-C) to noise variance. Then, assuming that the SNR is given, we can compute the corresponding noise variance.

We use the DOR scenario from Section II-C (averaged concentration distribution) as the source model, a circular array of radius r centered at the origin of coordinate system, and $\text{SNR} = 3$ dB. The sampling interval is $T_s = 1000$ s.

In Figs. 5 and 6, we present the probability of detection P_{d} for the GLR detector. Fig. 5 shows P_{d} as a function of the

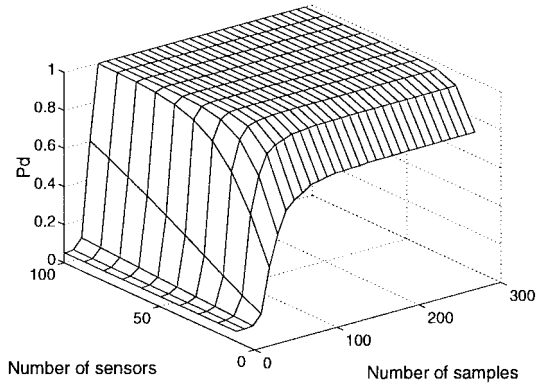


Fig. 5. Detection probability DOR scenario, $r = 2500$ m, for the GLR detector.

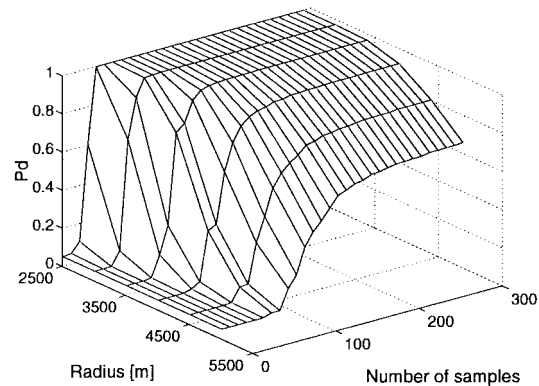


Fig. 6. Detection probability DOR scenario, $m = 100$, for the GLR detector.

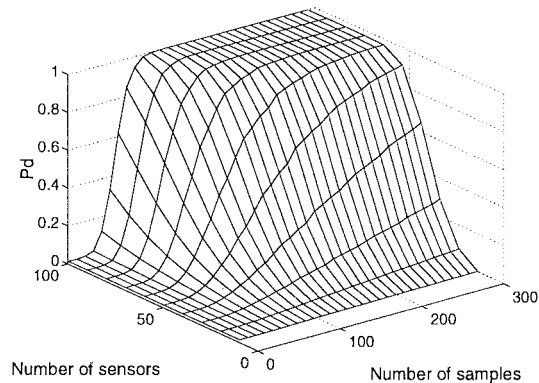


Fig. 7. Detection probability DOR scenario, $r = 2500$ m, mean detector.

number of sensors m and number of time samples p . Fig. 6 shows P_{d} as a function of p and r for $m = 100$.

For comparison purposes, in Figs. 7 and 8, we present the detection probability using the mean detector. As expected, the GLR detector gives a higher detection probability unless the number of sensors or time samples is large.

IV. SENSOR ARRAY DESIGN

We apply the above results on detection performance to optimally design the array of the sensors. The design is with respect to the system parameters defining the array

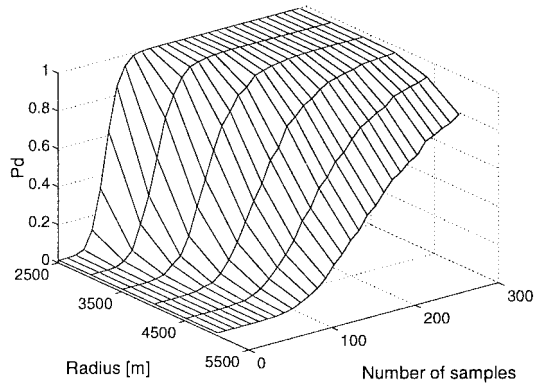


Fig. 8. Detection probability DOR scenario, $m = 100$, mean detector.

configuration: the array radius r , number of sensors m , and number of time samples p .

A. Detection Performance Criterion

We demonstrate how to select the array parameters to achieve a desired detection probability P_d^* for a fixed P_{fa} .

Since P_{fa} is fixed, the threshold τ is a function of m and p only, more precisely of mp [see (3.24) and (3.27)]. On the other hand, P_d is a function of the source parameters and array radius through the noncentrality factor λ [see (3.24) and (3.27)]. Therefore, the array parameters yielding P_d^* are found by solving (3.24) or (3.27) for fixed P_{fa} and SNR.

The procedure for selecting the array parameters can be summarized as follows.

- Set an acceptably small level of false alarm P_{fa} (e.g., 5–10%).
- Compute the corresponding threshold τ as a function of mp .
- For this τ , find combinations of m and p that give the desired P_d^* using (3.24) and (3.27). These values are obtained by finding the curve of intersection of the surface $P_d(m, p)$ with the (horizontal) plane $P_d(m, p) = P_d^*$.
- Repeat the previous step for different values of array radius.

As a result, we obtain a set of possible choices for the array parameters m , p , and r that guarantees the desired P_d^* . This set can be presented as a surface in three-dimensional (3-D) space, as will be shown in Section IV-C.

Using the above procedure, we design a detector that guarantees the required P_{fa} . However, P_d is calculated using an averaged concentration distribution, and, hence, for a particular set of source locations and intensities, P_d may be different from P_d^* .

B. Optimum Design

An optimum selection of the number of sensors m and number of time samples p can be done by minimizing a cost function C of involved system parameters, given the SNR, P_{fa} , and desired P_d^* . For example,

$$C = C_1 m + C_2 p \quad (4.28)$$

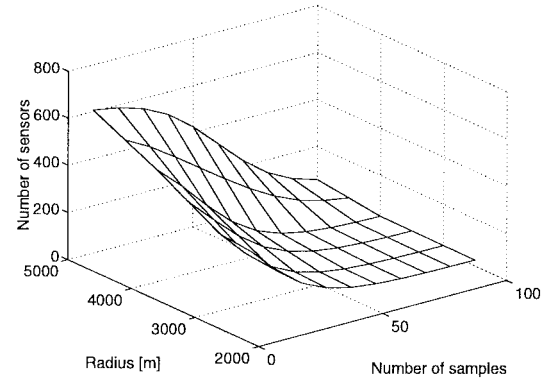


Fig. 9. System parameters to achieve $P_d^* = 95\%$ with the DOR scenario, GLR detector.

where C_1 is the cost per sensor and C_2 is the cost per time sample.

The optimal design, assuming the array radius r is fixed, is described by the following procedure.

- Use the same algorithm as in the previous section to find the set of candidate choices for m and p that give the desired P_d^* .
- Minimize C over that set.
- Repeat the previous steps for different values of r .

For any r , this procedure yields the optimal choice of m and p with a corresponding cost. Then, the final decision can be made by selecting the largest radius with acceptable cost.

The above optimization can be generalized to an unconstrained problem if P_{fa} and P_d are not restricted. Then C can be defined as

$$C = C_1 m + C_2 p + g_1(P_m) + g_2(P_{fa}) \quad (4.29)$$

where g_1 and g_2 are increasing functions of P_{fa} and P_m , respectively, and $P_m = 1 - P_d$ is the probability of “miss.”

Assuming that SNR is given, P_m can be expressed as a function of m , p , and P_{fa} through the threshold τ . Thus, the optimization problem reduces to finding m , p , and P_{fa} such that (4.29) is minimized.

C. Numerical Examples of Array Design

We present numerical examples of sensor array design for the DOR scenario Section II-C using the above procedure. In all examples, it is assumed that the sensors’ sensitivity threshold is sufficiently small, so that the detection performance is unaffected.

Figs. 9 and 10 illustrate the possible combinations of number of time samples, array radius, and number of sensors that yield detection probabilities $P_d^* = 95\%$ and $P_d^* = 99\%$, respectively. Any point on the surfaces shown in these figures will guarantee the required P_d^* and P_{fa} .

Fig. 11 shows the optimal number of sensors as a function of relative cost $C_r = C_p/C_m$. The array radius is fixed at $r = 2500$ m and $P_d^* = 95\%$. Similarly, Fig. 12 shows the corresponding number of samples. It can be seen that the optimum number of sensors (time samples) increases (decreases) with the relative cost of time samples versus the number of sensors.

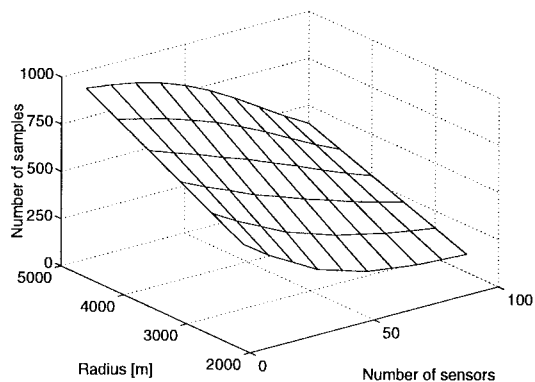
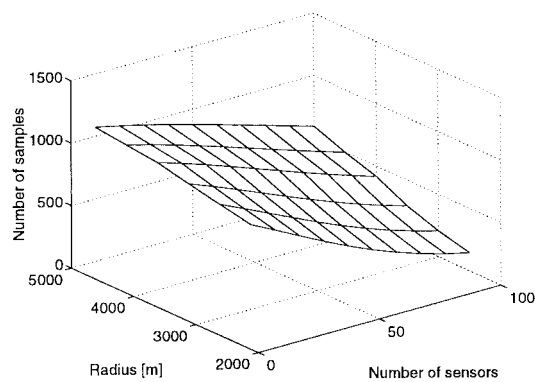
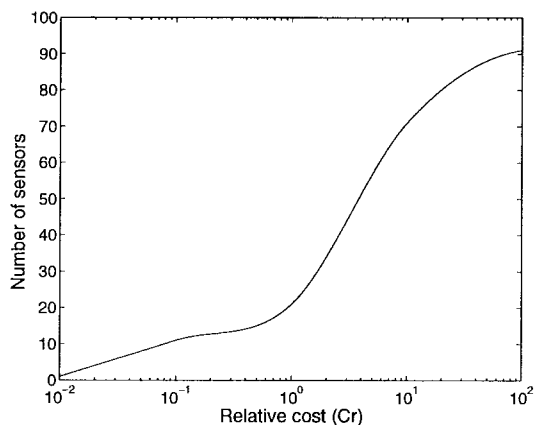
Fig. 10. System parameters to achieve $P_d^* = 99\%$, GLR detector.Fig. 13. System parameters to achieve $P_d^* = 95\%$, mean detector.

Fig. 11. Optimal number of sensors as a function of relative cost, GLR detector.

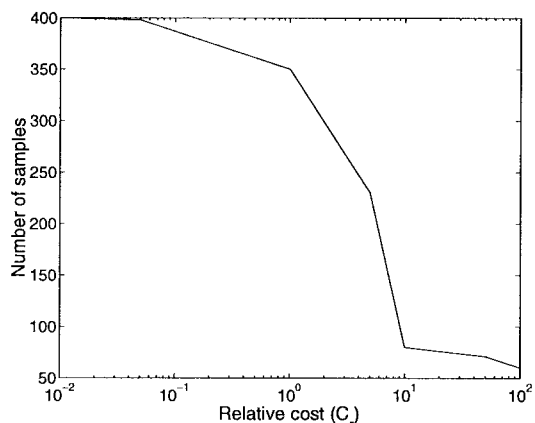


Fig. 12. Optimal number of time samples as a function of relative cost, GLR detector.

In Fig. 13, we show design results for the mean detector, $P_d^* = 95\%$. As expected, the number of time samples required to achieve the same detection performance is significantly larger compared with the GLR detector.

V. SUMMARY AND CONCLUDING REMARKS

We have proposed detection algorithms for environmental monitoring of disposal sites in the deep ocean using chemical sensor arrays. The algorithms included the GLR and mean

detectors. The GLR detector gives a higher performance and is applicable when the physical model is reliable, while the mean detector is useful when a precise model is not available. We have analyzed the performance of both detectors using the probability of detection P_d and false alarm P_{fa} . We have also proposed algorithms for optimal array design assuming a variety of performance and cost requirements. The design included selection of a number of sensors and time samples.

To ensure the applicability of the GLR test, it would be useful to examine the model assumptions by simulating a realistic disposal during a controlled research. The measurement vector obtained during this test could be used to model the transport of dissolved materials, i.e., to estimate parameters that cannot be measured such as eddy diffusivities.

The detection performance is also strongly affected by the source intensity model and, therefore, further experiments are required to obtain a model for the dewatering processes and to quantify the release rates.

An effort should be made to examine the robustness of the GLR detector. In practice, the actual parameter values may be different from those assumed in the model (3.12), alternatively the real measurement process may differ from (2.9). Therefore, deterioration in the detection performance due to parameter/model deviations should be investigated.

Equations (3.24) and (3.27) were derived under the assumption that the sensor noise can be modeled as a Gaussian process. Research should be undertaken to investigate changes in detection performance and array design for different noise models. This also indicates that an effort should be made to model the sensor noise more accurately.

The sensor array can be designed using either the GLR or mean detectors. However, if conditions are right, the GLR detector will perform much better than the mean detector, unless the number of samples is very large. In practice, the number of sensors used for the GLR detector should be larger than the numbers found in Section IV-B, to guarantee the desired performance level in the presence of potential modeling errors such as those discussed above.

Future research should also include improving detection performance by using flux (vector) sensors, decreasing detection time and computations by using an adaptive sampling rate, detection in the case of unknown medium parameters (deterministic and/or random), and extensions of the measurement

model to more realistic scenarios. Preliminary results for these extensions are presented in [17].

Finally, in order to ensure higher detectability at larger distances, more sensitive sensor technologies are required. This is true in particular for metal pollutants since existing sensors will most likely be unable to detect metals outside of the near-field area (see also [17]).

APPENDIX A

Using the transformation (2.2), the Cartesian form of (2.4) translates to

$$\frac{\partial c}{\partial t} = \kappa \left(\frac{\partial^2 c}{\partial x'^2} + \frac{\partial^2 c}{\partial y'^2} + \frac{\partial^2 c}{\partial z'^2} \right) - v'_x \frac{\partial c}{\partial x'} - v'_y \frac{\partial c}{\partial y'} - v'_z \frac{\partial c}{\partial z'} \quad (\text{A.1})$$

where we have used the facts that $\mathbf{v}' = \mathcal{K}\mathbf{v}$ and $(\partial c/\partial x = \partial c/\partial x')\sqrt{\kappa/\kappa_x}$, and similar expressions for the y and z components.

The above equation corresponds to an advective diffusion in isotropic media and therefore can be solved easily (see [3]). The solution can be obtained using a 3-D Fourier transformation with respect to the spatial coordinates (see [3]). It can be shown that the impulse response (Green's function) is given by

$$h(\mathbf{r}', t) = \frac{1}{[4\pi\kappa(t-t_0)]^{3/2}} \cdot \exp \left\{ -\frac{|\mathbf{r}' - \mathbf{v}(t)(t-t_0) - \mathbf{r}'_0|^2}{4\kappa(t-t_0)} \right\} \quad (\text{A.2})$$

where $\mathbf{r}' = \mathcal{K}\mathbf{r}$.

Then, the concentration in the presence of a point source with release rate $\mu(t)$ is given by the convolution integral

$$c(\mathbf{r}, t) = \int_{t_0}^t x(\tau) h(\mathbf{r}, t-\tau) d\tau \quad (\text{A.3})$$

where $\mu'(t) = \mu(t)/|K|$.

APPENDIX B

The coefficient c_l (3.24) is the probability that exactly l components of the vector $\hat{\boldsymbol{\mu}}$ are greater than zero. The probability that particular l components, for example, the first l , are greater than zero is

$$\int_0^\infty \cdots \int_0^\infty \int_{-\infty}^0 \cdots \int_{-\infty}^0 \frac{1}{(2\pi)^{n/2} |\Sigma|^{1/2}} \cdot \exp \left\{ -\frac{1}{2} (\mathbf{x} - \boldsymbol{\mu})^T \Sigma^{-1} (\mathbf{x} - \boldsymbol{\mu}) \right\} d\mathbf{x} \quad (\text{B.1})$$

where $\Sigma = \sigma(A'A)^{-1}$. Using the transformation $\mathbf{z} = \Sigma^{-1/2}(\mathbf{x} - \boldsymbol{\mu})$, (B.1) becomes

$$\int_{u_1}^\infty \cdots \int_{u_l}^\infty \int_{-\infty}^{u_{l+1}} \cdots \int_{-\infty}^{u_n} \frac{1}{(2\pi)^{n/2}} \exp \left\{ -\frac{\mathbf{z}^T \mathbf{z}}{2} \right\} d\mathbf{z} \quad (\text{B.2})$$

where $u_l = \mathbf{h}_l^T \boldsymbol{\mu}$ and \mathbf{h}_l are the columns of $\Sigma^{-1/2}$, i.e.,

$$\Sigma^{-1/2} = [\mathbf{h}_1 \cdots \mathbf{h}_n]. \quad (\text{B.3})$$

Then, c_l is given as a sum of probabilities for all possible realizations

$$c_l = \sum_{i_1 \cdots i_n} \prod_{j=1}^n w_j^{i_j} (1-w_j)^{1-i_j} \quad (\text{B.4})$$

$$w_j = \text{erfc}(\mathbf{h}_j^T \boldsymbol{\mu}) \quad (\text{B.5})$$

$$i_1 \cdots i_n \in \{0, 1\} \quad \text{and} \quad i_1 + \cdots + i_n = k. \quad (\text{B.6})$$

APPENDIX C

The GLR test (3.22) is distributed as

$$\text{GLR} = \begin{cases} 1, & l = 0 \\ F_{l, mp-l}(\lambda), & 1 < l \leq n \end{cases} \quad (\text{C.1})$$

with

$$\lambda = \begin{cases} 0, & \text{under } H_0 \\ \frac{\boldsymbol{\mu}^T A^T A \boldsymbol{\mu}}{\sigma^2}, & \text{under } H_1. \end{cases} \quad (\text{C.2})$$

Performance measures are then given by

$$P_{\text{fa}} = \Pr[\text{GLR} > \tau | H_0] = \sum_{l=0}^n \Pr[F_{l, mp-l}(0) > \tau | L=l] \Pr[L=l] \quad (\text{C.3})$$

$$P_{\text{d}} = \Pr[\text{GLR} > \tau | H_1] = \sum_{l=0}^n \Pr[F_{l, mp-l}(\lambda) > \tau | L=l] \Pr[L=l]. \quad (\text{C.4})$$

ACKNOWLEDGMENT

The authors would like to thank the organizers of and participants in the DOR Phase II Project, in particular Dr. P. Fleischer, Dr. A. Green, Dr. R. Jahnke, Dr. J. Proni, Dr. D. Rhoads, Dr. P. Valent, and Dr. D. Young, for providing valuable information and comments on the DOR model.

REFERENCES

- [1] P. J. Valent and D. K. Young, "Abyssal seafloor waste isolation: Environmental report," Naval Research Laboratory, Stennis Space Center, MS, NRL/MR/7401-95-7576, Sept. 1995.
- [2] A. Jeremić and A. Nehorai, "Design of chemical sensor arrays for monitoring disposal sites on the ocean floor," in *Proc. IEEE ICASSP*, May 1998, vol. 4, pp. 2013-2016.
- [3] A. Nehorai, B. Porat, and E. Paldi, "Detection and localization of vapor-emitting sources," *IEEE Trans. Signal Processing*, vol. 43, pp. 243-253, Jan. 1995.
- [4] H. L. Van Trees, *Detection, Estimation, and Modulation Theory; Part I*. New York: Wiley, 1968.
- [5] "Draft environmental impact report," Berth Dredging Project, Boston, MA, EDEA File 8695, Apr. 1994.
- [6] D. Rhoads, "Sensor requirements for a temporally tiered compliance monitoring program," Science Applications International Corp., Newport, RI, SAIC Doc. 97-12, May 1997.
- [7] J. R. Proni and T. A. Nelsen, "Impact plume monitoring," Naval Research Laboratory, Stennis Space Center, MS, DOR Subgroup Rep., DOR Phase II minutes of Oct. 15-18 meeting, Oct. 1996.
- [8] P. C. Gallacher, P. Pistek, and A. Green, "Hydrodynamical dispersion of dredged materials sequestered on the abyssal plains," *J. Marine Syst.*, submitted for publication.

- [9] A. Okubo, "Horizontal and vertical mixing in the sea," in *Impinging of Man on the Oceans*, D. W. Hood, Ed. New York: Wiley Interscience, 1971, pp. 89–167.
- [10] J. Crank, *The Mathematics of Diffusion*. Oxford, U.K.: Oxford Univ., 1956.
- [11] G. Matisoff, "Mathematical models of bioturbation," in *Animal-Sediment Relations*, P. L. McCall and M. J. S. Tevesz, Eds. New York: Plenum, 1982, Geobiology Series, vol. 2, pp. 289–330.
- [12] G. Kullenberg, *Pollutant Transfer and Transport in the Sea*. Boca Raton, FL: CRC Press, 1982, vols. I and II, 1982.
- [13] T. Beer, *Environmental Oceanography: An Introduction to the Behavior of Coastal Waters*. New York: Pergamon, 1983.
- [14] R. A. Jahnke, "Monitoring contaminants release and transport from dredged material stored on the abyssal seafloor," Naval Research Laboratory, Stennis Space Center, MS, DOR Subgroup Report, DOR Phase II minutes of Feb. 19–20 meeting, Feb. 1996.
- [15] A. Green, "Dynamics of GFC's in free-fall," Naval Research Laboratory, Stennis Space Center, MS, Feb. 19–20, 1997, (DOR Phase II minutes of Feb. meeting).
- [16] P. Fleischer, F. A. Bowles, and M. D. Richardson, "Geo-fabric container monitoring: Dewatering and other physical changes occurring in GFC's relocated on the abyssal sea floor," Naval Research Laboratory, Stennis Space Center, MS, DOR Phase II minutes of May 21–22 meeting, May 1997.
- [17] A. Nehorai and A. Jeremić, "Design of chemical sensor for monitoring dredge disposal sites on the ocean floor," Dept. of Electrical Engineering and Computer Science, Univ. of Illinois at Chicago, Chicago, IL, Rep. UIC-EECS-97-7, May 1997.
- [18] T. W. Anderson, *An Introduction to Multivariate Statistical Analysis*, 2nd ed. New York: Wiley, 1984.
- [19] C. L. Lawson and R. J. Hanson, *Solving Least Squares Problems*. Englewood Cliffs, NJ: Prentice-Hall, 1974.
- [20] H. V. Poor, *An Introduction to Signal Detection and Estimation*, 2nd ed. New York: Springer-Verlag, 1994.
- [21] L. Scharf and B. Friedlander, "Matched subspace detectors," *IEEE Trans. Signal Processing*, vol. 42, pp. 2146–2157, Aug. 1994.
- [22] J. C. Kiefer, *Introduction to Statistical Inference*. New York: Springer-Verlag, 1987.
- [23] C. R. Rao, *Linear Statistical Inference and Its Applications*, 2nd ed. New York: Wiley, 1973.



Aleksandar Jeremić (S'97) received the B.Sc. degree in electrical engineering from the University of Belgrade in 1995 and the M.Sc. degree in electrical engineering from the University of Illinois at Chicago in 1997. He is working toward the Ph.D. degree at the Department of Electrical Engineering and Computer Science at the University of Illinois at Chicago.



Arye Nehorai (S'80–M'83–SM'90–F'94) received the B.Sc. and M.Sc. degrees in electrical engineering from the Technion–Israel Institute of Technology in 1976 and 1979, respectively, and the Ph.D. degree in electrical engineering from Stanford University, Stanford, CA, in 1983.

After graduation, he was a Research Engineer at Systems Control Technology, Inc., Palo Alto, CA. From 1985 to 1995, he was with the Department of Electrical Engineering, Yale University, New Haven, CT, where he became an Associate Professor in 1989. In 1995, he joined the Department of Electrical Engineering and Computer Science of The University of Illinois at Chicago (UIC) as a Full Professor. He holds a joint professorship with the Bioengineering Department at UIC. He is an Associate Editor of *Circuits, Systems, and Signal Processing* and *The Journal of the Franklin Institute*.

Dr. Nehorai is an Associate Editor of the IEEE TRANSACTIONS ON ANTENNAS AND PROPAGATION, the IEEE JOURNAL OF OCEANIC ENGINEERING and has been Associate Editor of the IEEE TRANSACTIONS ON ACOUSTICS, SPEECH AND SIGNAL PROCESSING. He served as Chairman of the Connecticut IEEE Signal Processing Chapter from 1986 to 1995 and is currently Vice-Chair of the IEEE Signal Processing Society's Technical Committee on Sensor Array and Multichannel (SAM) Processing. He was co-recipient, with P. Stoica, of the 1989 IEEE Signal Processing Society's Senior Award for Best Paper. He is a fellow of the Royal Statistical Society.